Inorganic Chemistry

Article

pubs.acs.org/IC

Crystalline and Liquid Structure of Zinc Chloride Trihydrate: A Unique Ionic Liquid

Robert J. Wilcox,[†] Bradley P. Losey,[†] Jacob C. W. Folmer,[†] James D. Martin,*[,†] Matthias Zeller,[‡] and Roger Sommer[†]

[†]Department of Chemistry, North Carolina State University, Raleigh, North Carolina 27695-8204, United States

[‡]Department of Chemistry, Youngstown State University, Youngstown, Ohio, 44555, United States

Supporting Information

ABSTRACT: The water/$ZnCl_2$ phase diagram in the vicinity of the 75 mol % water composition is reported, demonstrating the existence of a congruently melting phase. Single crystals of this 3-equiv hydrate were grown, and the crystal structure of $[Zn(OH_2)_6][ZnCl_4]$ was determined. Synchrotron X-ray and neutron diffraction and IR and Raman spectroscopy along with reverse Monte Carlo modeling demonstrate that a CsCl-type packing of the molecular ions persists into the liquid state. Consistent with the crystalline and liquid structural data, IR spectroscopy demonstrates that the O−H bonds of coordinated water do not exhibit strong intermolecular hydrogen ion bonding but are significantly weakened because of the water's coordination to Lewis acidic zinc ions. The O−H bond weakening makes this system a very strong hydrogen-bond donor, whereas the ionic packing along with the nonpolar geometry of the molecular ions makes this system a novel nonpolar, hydrogen-bonding, ionic liquid solvent.

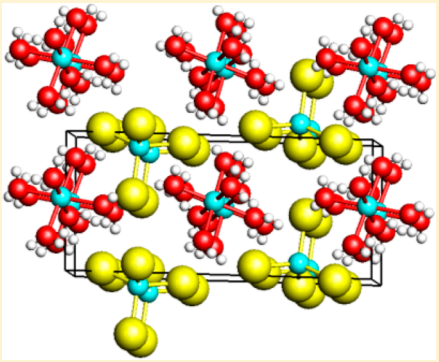

INTRODUCTION

Zinc chloride hydrate has been of considerable interest for various applications, as well as the subject of countless basic science investigations probing the nature of the solutes and solvent, particularly in concentrated solutions. More than 150 years ago, it was discovered that concentrated zinc chloride hydrates are an effective solvent for cellulose.[1] Zinc chloride hydrates are instrumental for the formation and transport of hydrothermal ores.[2,3] Zinc chloride hydrate solutions are ubiquitous for electroplating (galvanization) and are important in battery applications.[4] Hydrolyzing zinc chloride hydrates is important for dental cement.[5] Zinc plays numerous important roles in biology.[6,7] Better knowledge of the extent in which both chloride ions and water molecules are associated with the zinc ion is critical to both the fundamental understanding and effective application of these systems. This, in turn, may lead to a better understanding of the role of this important micronutrient in biology.

Hydrates of zinc chloride afford one of the largest concentration ranges over which a salt hydrate system is liquid at room temperature. At 25 °C, $ZnCl_2$ exhibits a solubility of 432 g/100 mL of H_2O (R = 1.75; 64 mol % H_2O; 31 m). (R has been used to describe the number of equivalents of water per equivalent of zinc.) In his 1968 review, Braunstein divided aqueous salt solutions into five classes defined by approximate ranges of water mole fraction: (I) Debye−Hückel limiting (1 to >0.99); (II) extended Debye−Hückel theory (0.99−0.9); (III) hydrate melts (0.9−0.75); (IV) incomplete hydration sheaths (0.75−0.01); (V) gas solubility (<0.01).[8] Braunstein noted that solutions with concentrations between about 1 and 80 mol % water are of particular interest, where "the hydration shells of the ions must be incomplete and one must consider ion−ion, water−water and water−ion interactions." As demonstrated by the $ZnCl_2/H_2O$ phase diagram,[9,10] four of the five Braunstein classes of hydrates are liquid at room temperature in this system. Additionally, there are likely several hydrate phases that crystallize with discrete compositions below room temperature. Numerous measurements of the physical properties including for electromagnetic force,[11−15] conductivity,[16−22] vapor pressure,[13,14,16] density,[18] viscosity,[18,20,23] relaxation time for water exchange,[24] and glass transition temperatures[11,20] of zinc chloride hydrates across the concentration ranges of type II and III solutions indicate a variety of anomalies that suggest the likelihood of concentration-controlled structural variation in the liquid hydrate phases. Any such structural variation is most likely accounted for by ion association and/or organization of the waters of solvation.

An extensive set of Raman[24−27] and X-ray absorption spectroscopy[28,29] and X-ray (XRD) and neutron diffraction[26] studies have probed the solution structure and ion speciation of zinc chloride hydrates. Various theoretical studies have further attempted to bring clarity to the nature of hydrated species present.[34,35] There is a clear consensus that, in the presence of excess chloride, the $ZnCl_4^{2-}$ anion is the most prevalent zinc-containing species. However, there is significant variation in

Special Issue: To Honor the Memory of Prof. John D. Corbett

Received: October 6, 2014
Published: January 17, 2015

DOI: 10.1021/ic5024532
Inorg. Chem. 2015, 54, 1109−1119

species proposed to account for the data measured for the pure zinc chloride hydrates. Possible tetrahedral $[ZnCl_n(OH_2)_{4-n}]^{2-n}$ (n = 1−4) and octahedral $[ZnCl_n(OH_2)_{6-n}]^{2-n}$ (n = 0−4) species have been proposed. The strong Raman peak at ∼280 cm^{-1}, observed across an extensive range of concentrations, is characteristic of the $ZnCl_4^{2-}$ anion, although there is some debate as to whether this is actually $[ZnCl_4(OH_2)_2]^{2-}$.[24−27] Similarly, the peak observed at ∼390 cm^{-1}, consistent with that observed for solutions of zinc perchlorate,[36] is assigned to $Zn(OH_2)_6^{2+}$. Attempts to appropriately fit peak shapes, however, have led to the suggestion of other mixed chloride/hydrate species.

Diffraction studies of concentrated solutions all imply that zinc is coordinated to both chloride and water ligands, albeit with some difference of perspective as to whether the total zinc coordination number is 4 or 6.[26,30−33] A $^{35}Cl/^{37}Cl$ neutron diffraction study further indicated that the coordination number around chloride is 5.6 in dilute solutions (<0.47 m; R > 100) and decreases to 4.4 in more concentrated (4 m; R = 13) solutions.[33] It is interesting to observe that, in the Raman studies, authors accounted for the seemingly conflicting coordination information by proposing a variety of speciations. By contrast, diffraction studies tend to consider the data to be reflective of a single zinc environment. The latter requires that there is some degree of oligomerization in which chlorides are shared between zinc atoms.[30] In very concentrated solutions, >10 M (18.5 m; R = 3), both Irish et al.[24] and Yamaguchi et al.[26] also suggest Raman spectroscopic evidence for oligomeric speciation.

Precedence for a variety of the proposed chloride/hydrate species can be found from single-crystal structures of ternary systems. In combination with alkali cations, zinc chloride hydrates yield, for example, the tetrahedral $ZnCl_4^{2-}$ anion in the crystalline structure of $Li_2ZnCl_4{\cdot}2H_2O$, with the waters being uniquely associated with the Li^+ cations,[37] and the pseudotetrahedral $[ZnCl_3(OH_2)]^-$ ion in $KZnCl_3{\cdot}2H_2O$.[38] In the presence of large macromolecules such as the 18-crown-6 macrocycle, a neutral pseudotetrahedral species $ZnCl_2(OH_2)_2$ is observed.[39] A search of the Cambridge Structural Database and Inorganic Crystal Structure Database finds no examples of zinc monochloride hydrate. The only single-crystal structure of a binary zinc chloride hydrate, prior to this work, is $ZnCl_2{\cdot}1.33$ H_2O in which two-thirds of the zinc atoms form polymeric chains, tetrahedrally coordinated by bridging chlorides, and the remaining one-third of the zinc atoms are octahedrally coordinated with four independent water molecules and two chlorides, shared with the aforementioned polymeric chains.[40]

Given our interest in understanding and designing the structure in materials at the crystalline/liquid (amorphous) interface, which we previously achieved in inorganic networks using templating organic cations,[41,42] we were drawn to the zinc chloride hydrate system as one in which significant amorphous structure might be engineered without the inclusion of organic templates. Reinvestigation of the water/zinc chloride phase diagram identifies the 3-equiv hydrate (R = 3; 18.5 m; 10.1 M) to be a congruently melting phase. Here we report the single-crystal structure of this hydrate and demonstrate by synchrotron XRD and variable-temperature neutron diffraction, along with reverse Monte Carlo (RMC) modeling, the high degree of structural correlation between the liquid and crystalline phases. Examination of the IR water spectrum further demonstrates the hydrogen-bonding capacity of this novel ionic liquid.

RESULTS

$(H/D)_2O/ZnCl_2$ Phase Diagram. The most complete previously reported water/$ZnCl_2$ phase diagram is that of Mylius and Dietz in 1905,[9] i.e., prior to the discovery of XRD. It gives an indication of several potentially crystalline zinc chloride hydrate phases, although their crystalline structures are unconfirmed. Using doubly sublimed anhydrous $ZnCl_2$ and 18 MΩ H_2O or as purchased 99.99% D_2O, we initiated a careful reexamination of this phase diagram by differential scanning calorimetry (DSC), gravimetric analysis, synchrotron XRD and neutron diffraction, and Raman and IR spectroscopy. Shown in Figure 1 is the portion of the phase diagram surrounding the R = 3 [75 mol % $(H/D)_2O$] composition. These data demonstrate the existence of a congruently melting phase at the R = 3 composition, with no significant evidence of any solid solution formation. The H_2O compound exhibits a melting point of 6 °C, whereas the melting point for the D_2O compound is −1 °C. It is interesting to note that this water/zinc chloride system exhibits an inverse isotope effect compared to that of water for which H_2O melts at 0 °C and D_2O melts at 3.8 °C.

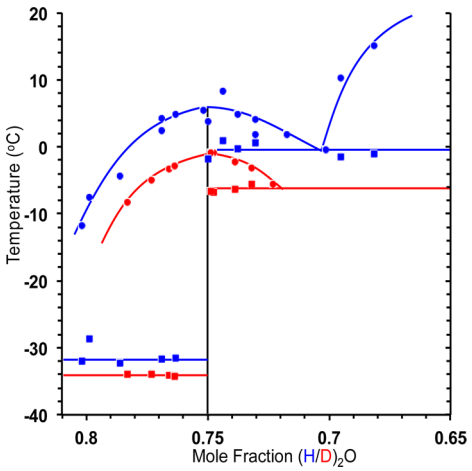

Figure 1. Water/zinc chloride phase diagram in the vicinity of the R = 3 composition. Data for H_2O are plotted in blue, and data for D_2O are plotted in red.

Structure of $[Zn(O(H/D)_2)_6][ZnCl_4]$, I_H and I_D. In other work in our laboratory, we have determined that for congruently melting materials it is often possible to access conditions in which crystal nucleation is slow but growth is fast, conditions necessary for single-crystal growth, by rapidly quenching a molten sample to an isotherm 5−50 °C below the melting point.[43,44] Single-crystal growth is further facilitated by limiting the total volume of the sample being crystallized, such as within a capillary. Applying this crystallization technique to the R = 3 zinc chloride molten salt hydrate resulted in successful single-crystal growth upon quenching to 253 or 223 K isotherms. Data for three separate in situ grown single crystals of the H_2O compound ($\mathbf{I_H}$) were collected after cooling the crystal to 254, 208, and 100 K and for single crystals of the D_2O compound ($\mathbf{I_D}$) at 233 K. A summary of the crystallographic data is given in Table 1. Full details of the structure solutions are available in the Supporting Information (SI).

Of the three $\mathbf{I_H}$ single crystals examined, the one for which data were collected at 208 K was of the highest quality and thus

DOI: 10.1021/ic5024532
Inorg. Chem. 2015, 54, 1109−1119

Table 1. Single-Crystal Data and Refinement Parameters for $[Zn(O(H/D)_2)_6][ZnCl_4]$

empirical formula	$Zn_2Cl_4O_6H_{12}$			$Zn_2Cl_4O_6D_{12}$
fw	380.68			392.71
cryst color	colorless			
cryst syst	triclinic			
space group	$P\bar{1}$			
temperature, K	100	208	254	233
a, Å	6.413(3)	6.4421(15)	6.477(3)	6.4728(9)
b, Å	6.506(3)	6.5034(15)	6.511(3)	6.5054(8)
c, Å	14.211(6)	14.281(3)	14.291(7)	14.2949(18)
α, deg	90.946(3)	90.626(3)	90.466(8)	90.656(3)
β, deg	99.278(7)	99.082(3)	98.900(8)	98.936(3)
γ, deg	95.741(7)	95.490(3)	95.575(8)	95.498(3)
V, Å^3	581.9(4)	587.9(2)	592.4(5)	591.77(13)
Z	2	2	2	2
R ($F^2 > 2\sigma F^2$)	0.085	0.046	0.079	0.0223
R_w	0.190	0.128	0.184	0.0536
GOF	1.064	1.110	1.071	1.034

is the one from which distance information is reported throughout this manuscript. Other than thermal expansion for which the unit-cell volume increases by about 0.066 Å^3·K^{-1} (see Figure S1 in the SI), the crystal structure is equivalent for each of the temperatures examined. The heavy atom arrangement in the $\mathbf{I_D}$ single-crystal structure is equivalent to that of the $\mathbf{I_H}$ structure but with some variation in the H/D positions. In the structure solutions, all heavy atoms were clearly located in the difference maps. Hydrogen atoms were tentatively assigned from difference density Fourier maps. For $\mathbf{I_H}$, the O−H distances were then constrained to 0.84(2) Å, the H−H distances within each water molecule were constrained to 1.35(2) Å, and U_{iso}(H) was set to 1.5U_{eq}(O) of the adjacent oxygen atom. For $\mathbf{I_D}$, the O−D distances were then constrained to 0.95(2) Å, based on pair distribution function (PDF) analysis of the neutron diffraction data, and 1.5U_{iso}(D) was set to U_{eq}(O) of the adjacent oxygen atom.

Powder neutron diffraction data were collected on multiple samples of $\mathbf{I_D}$, crystallized using various cooling profiles, and quenched to slow cooling. Slow cooling (0.5 K/min) to 225 K yielded the most polycrystalline sample. The significant variation in the peak intensities in the diffraction patterns, even for the same sample crystallized under different cooling regimes, is likely a result of incomplete orientational randomization due to a small number of crystallites. A reasonable GSAS refinement was obtained from the most polycrystalline of these samples (see Figure S2 in the SI). The heavy-atom structure in this refinement is equivalent to the single-crystal X-ray structures, but accurate D positions were not obtained.

An ORTEP drawing of the R = 3 $\mathbf{I_H}$ crystal structure is given in Figure 2. The crystal structure consists of a cesium chloride type packing of hexaaquozinc cations and tetrachlorozincate anions, a structure isomorphous to the previously reported $[Mg(OH_2)_6][ZnCl_4]$.[45] A summary of intra- and intermolecular distances for the molecular ions is given in Tables 2 and 3. Two crystallographically distinct hexaaquozinc cations are observed, each located on centers of inversion. The orientation of the water molecules appears to be most strongly determined by their arrangement about the central zinc atom of the hydrated cation. Only weak hydrogen bonding is observed between neighboring hexaaquozinc cations, with the shortest O−O contact being 3.14 Å (see Table 3). Because the chloride

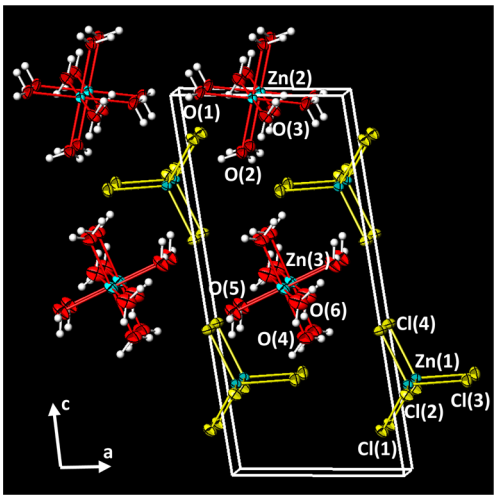

Figure 2. ORTEP drawing of R = 3 $[Zn(OH_2)_6][ZnCl_4]$ showing the crystallographic labeling scheme.

Table 2. Selected Bond Distances (Å) Observed for $[Zn(OH_2)_6][ZnCl_4]$ at 208 K

Zn−Cl	2.24−2.29
Zn−O	2.04−2.10
Cl−Cl$_{intra}$	3.61−3.81
Cl−Cl$_{inter}$	3.44−4.11 (4.70−5.80)
O−O$_{intra}$ cis	2.89−3.09
O−O$_{intra}$ trans	4.07−4.20
O−O$_{inter}$	3.09−3.55
Zn$_{Cl}$−Zn$_{O}$	5.01−7.19

Table 3. Nearest Intermolecular Ion Cl−O and O−O Contacts (Å) Observed for $[Zn(OH_2)_6][ZnCl_4]$ at 208 K

	Cl(1)	Cl(2)	Cl(3)	Cl(4)	
O(1)	3.17, 3.32	3.27, 3.73			O(1)−O(1) = 3.20
O(2)	3.55, 4.08	3.24, 3.68	3.26		O(2)−O(4) = 3.47
O(3)	3.23, 3.37, 4.04	3.71	3.35		O(3)−O(3) = 3.19
O(4)		3.36	3.43, 3.96	3.30	O(4)−O(2) = 3.47
O(5)		3.23		3.23, 3.69, 3.80	O(5)−O(5) = 3.61
O(6)			3.25	3.31, 3.69, 4.04	O(6)−O(6) = 3.14

coordination environment has been of interest to the study of molten salt hydrates,[33] all Cl−OH_2 contacts were analyzed and are summarized in Table 3. Each chloride has four to six water molecule neighbors with a Cl−O distance of less than 4.0 Å, filling a coordination hemisphere opposite to the Zn−Cl bond. However, there is no apparent strong geometric preference to the water−Cl interactions. Only limited weak hydrogen bonding to the tetrachlorozincate anion can be implied with only one contact below 3.2 Å but several contacts between 3.2 and 3.3Å ($\Sigma_{Cl-O\ vdw}$ = 3.3 Å).

Diffraction of the Molten Hydrate. To understand the relationship between the crystalline and molten hydrate phases, room temperature synchrotron and variable-temperature neutron diffraction data were obtained for the R = 3 hydrate. Structure factor plots of synchrotron XRD, R = 3 melt, as well as R = 1.7, water and molten $ZnCl_2$ (320 °C), and neutron R =

DOI: 10.1021/ic5024532
Inorg. Chem. 2015, 54, 1109−1119

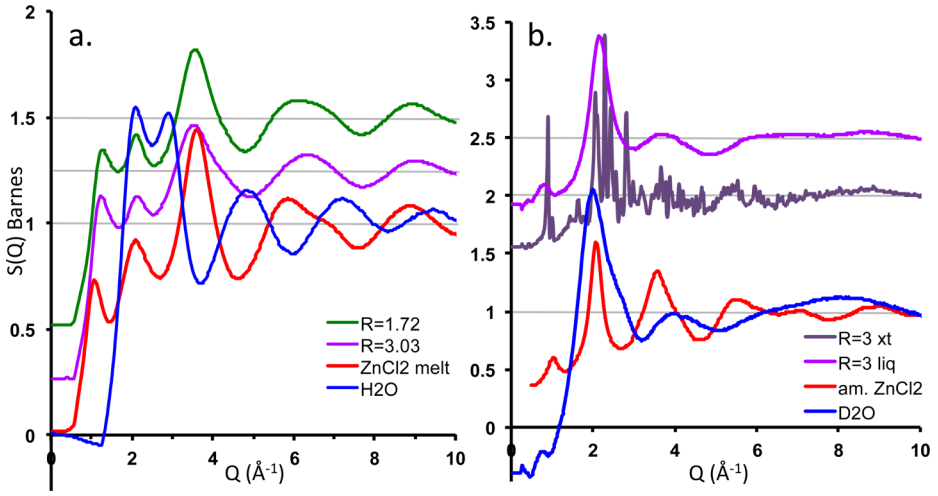

Figure 3. Structure factor plots of (a) the X-ray scattering of the room temperature molten hydrates R = 3 (purple), R = 1.7 (green), water (blue), and molten $ZnCl_2$ at 320 °C (red) and (b) the neutron scattering of the room temperature R = 3 molten hydrate (purple), 225 K R = 3 crystalline phase (dark purple), D_2O (blue), and amorphous $ZnCl_2$ (red).

3 melt (298 K) and crystal (225 K), as well as D_2O (298 K) and glassy $ZnCl_2$ (298 K) scattering are shown in Figure 3. Grossly, the structure factor plots of the R = 3 and 1.7 hydrates are very similar to that of molten anhydrous $ZnCl_2$. The most notable difference is observed for the lowest Q peak(s). In the X-ray data, this peak shifts from 1.07 $Å^{-1}$ for anhydrous molten $ZnCl_2$ to 1.28 and 1.23 $Å^{-1}$ for the R = 1.7 and 3 hydrates, respectively. In the neutron data, this peak shifts from 1.02 $Å^{-1}$ for the room temperature glassy $ZnCl_2$ to 0.81 $Å^{-1}$ for the R = 3 hydrate. The higher-Q peaks at ∼2.1 and ∼3.6 $Å^{-1}$ are remarkably similar across all of the zinc chloride based materials but clearly contrast with those of water. A comparison of the structure factor obtained for D_2O with literature reports suggests that the shoulder on the high Q side of the peak at 2.0 $Å^{-1}$ is indicative of some H_2O contamination in D_2O.[46]

To verify that there are no intermediate phases between **I** and the melt, variable-temperature neutron diffraction data were obtained in 1 K intervals between 255 and 280 K. As is visible in Figure S3 in the SI, melting is complete over a 1−2 K interval, with no evidence of any intermediate phases. This supports the DSC data in the phase diagram in Figure 1, which implied that the R = 3 material is congruently melting.

Raman Spectroscopy of the Molten Salt Hydrate. The Raman spectra of zinc chloride hydrates have been extensively studied.[24−27] As described in previous work, we find that the R = 3 hydrate spectrum is dominated by strong absorption at 286 cm^{-1} assigned to the symmetric stretch of the tetrahedral $ZnCl_4^{2-}$ anion (Figure S4 in the SI). The much weaker absorption at 390 cm^{-1} is consistent with the symmetric stretch of the octahedral $Zn(OH_2)_6^{2+}$ cation. Although not discussed in previous studies and presumably being treated as background, we observe that these peaks are superimposed on a strong luminescence. This luminescence dramatically increases for systems more concentrated than the eutectic composition at R ∼ 2.4 and decreases to negligible as R increases beyond 3, as will be reported in greater detail in a subsequent manuscript describing the full phase diagram.

Attenuated Total Reflection Infrared (ATR-IR) Spectroscopy of the Water of Hydration. The IR spectrum of 18 MΩ H_2O, as well as that of the R = 3 and 2 molten hydrates, is given in Figure 4. In the molten hydrates, the ν_{HOH} bend sharpens, increases in intensity, and red-shifts from 1638 cm^{-1} in bulk H_2O to 1617 and 1614 cm^{-1} for the R = 3 and 2 solutions, respectively. These spectra are not normalized with respect to the mole fraction of water. The maximum of the ν_{OH} stretching blue shifts from 3362 cm^{-1} in bulk H_2O to 3414 and 3410 cm^{-1} in the R = 3 and 2 solutions, respectively. The shoulder to the low-energy side of this peak (identified by the minimum in the first derivative of the spectrum), assigned as an overtone of the bending vibration and a result of network hydrogen bonding,[47] is significantly reduced in intensity and red-shifted from 3285 cm^{-1} in bulk H_2O to 3230 and 3225 cm^{-1} for the R = 3 and 2 solutions, respectively. The much weaker broad peak at ∼2120 cm^{-1} in bulk H_2O, a combination of libration, ν_{lib} (<650 cm^{-1}), and the ν_{HOH} bending modes, a consequence of a collective of many water molecules, is split into two broad peaks at 2290 and 2000 cm^{-1} for R = 3 and 2280 and 1990 cm^{-1} for R = 2 solutions. A dilution series finds that the 2120 cm^{-1} peak of bulk water is red-shifted, while the higher-energy peak grows in with increasing zinc chloride concentration. This higher-energy peak begins as a shoulder to the main peak at high dilution, achieving approximate parity in

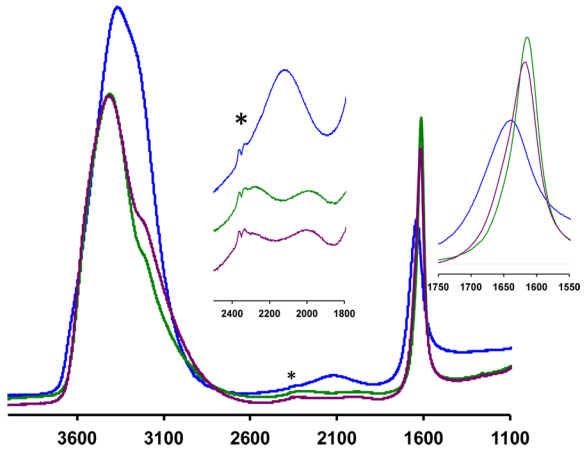

Figure 4. ATR-IR spectra of the R = 3 (purple) and 2 (green) zinc chloride hydrates, compared with that of 18 MΩ H_2O (blue). Insets: splitting of the band at ∼ 2100 cm^{-1} and shift of the ν_{HOH} bend, respectively. The asterisk indicates a trace of CO_2 in the spectrometer's beam path.

DOI: 10.1021/ic5024532
Inorg. Chem. 2015, 54, 1109−1119

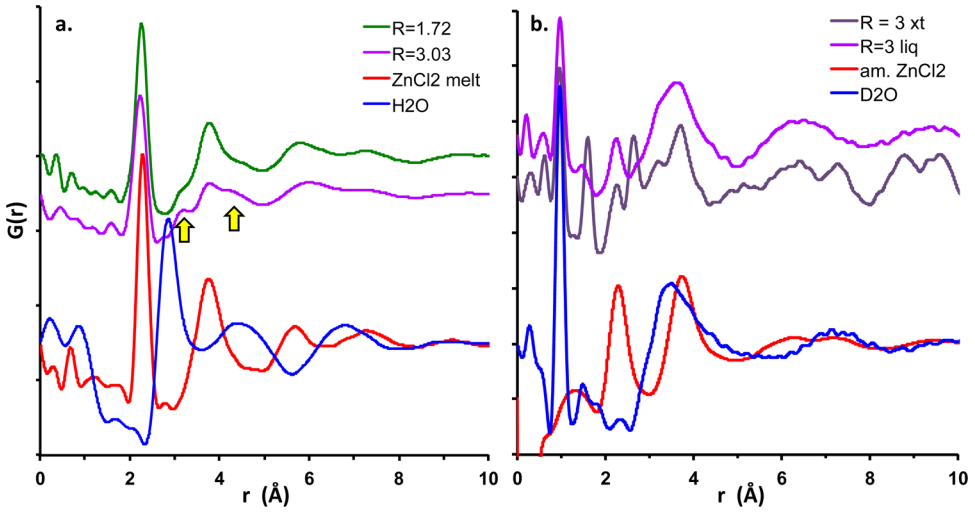

Figure 5. PDF plots of (a) the X-ray scattering of the room temperature molten hydrates R = 3.03 (purple), R = 1.72 (green), 18 MΩ H_2O (blue), and molten anhydrous $ZnCl_2$ at 320 °C (red) and (b) the neutron scattering of the room temperature R = 3 molten hydrate (purple), R = 3 crystals at 233 K (dark purple), D_2O (blue), and amorphous $ZnCl_2$ (red). Yellow arrows denote pair correlations previously assigned to zinc chloride oligomers but instead include O−O, Cl−O, Zn−Cl, and Zn−O pair correlations.

the R = 3 composition and becoming the more intense of the two in the R = 2 spectrum.

DISCUSSION

Crystalline Structure of I. One of the most significant features of the crystalline structure of **I** is the ligand partitioning such that there are two distinct zinc coordination environments: one coordinated exclusively by water and the other exclusively by chloride. That such ligand-sphere differentiation is observed might have been predicted based on the crystalline structure of the R = 1.33 hydrate in which the waters of hydration are restricted to only one-third of the zinc cations, with the remaining two-thirds of the zinc atoms being coordinated exclusively to chloride, forming $[Zn_2Cl_6]^{2-}$ polymeric chains.[40] In fact, we are finding that, even under dilute conditions, in the presence of chloride there is a strong preference for aqueous Zn^{2+} to form the $ZnCl_4^{2-}$ anion. The strong chlorophilicity of zinc must be a result of the relatively strong covalency of the Zn−Cl bonding, which can be anticipated given that Si^{4+} and Zn^{2+} exhibit similar electronegativities; i.e., $ZnCl_4^{2-}$ is an analogue of $SiCl_4$. Further evidence of this is seen in the structure of $[Mg(OH_2)_6][ZnCl_4]$ in which the water is exclusively coordinated to the more oxophilic magnesium.[46]

As described in the Results section (Table 3), the relatively long intermolecular ion O−O and O−Cl distances indicate that only weak hydrogen bonding exists within the crystalline network. This contrasts with the strong hydrogen bonding observed in bulk water. Interestingly, while stronger O−D bonding in D_2O compared to the O−H hydrogen bonding in H_2O results in its melting point being 3.8° higher, $\mathbf{I_D}$ exhibits a 7° lower melting point than $\mathbf{I_H}$. Together, the intermolecular ion distances and the inverse isotope effect observed for the melting point demonstrate that hydrogen bonding does not provide the major organizing influence on the structure of **I**.

Instead, multiple levels of crystal-packing principles are required to understand the structural organization of the respective molecular ions in **I**. It is observed that the $[Zn(OH_2)_6]^{2+}$ cations and $[ZnCl_4]^{2-}$ anions are of similar size with respect to a spherical approximation of ionic radii (r ∼ 3.5−3.8 and 4.0−4.2 Å, respectively). The resulting radius ratio, from a simple perspective of packing of ionic spheres, is consistent with the observed CsCl-type packing of the molecular ions. The triclinic cell of crystalline **I** is essentially a stacked set of two CsCl-type cubes, stretched along the c axis because of the shape and orientation of the $[ZnCl_4]^{2-}$ anions (Figure 2). At a finer level of structural analysis, it is observed that the chlorides of $[ZnCl_4]^{2-}$ are oriented such that they adopt approximately cubic-close-packed (ccp) positions (see Figure S5 in the SI). The water ligands are too small, and the $[Zn(OH_2)_6]^{2+}$ cations are too large to perfectly fill the holes of the pseudo-ccp layers. As a result, some combination of single water ligands, pairs of water ligands, or the entire $[Zn(OH_2)_6]^{2+}$ ions fill close-packed positions. It is also observed that the octahedral $[Zn(OH_2)_6]^{2+}$ cations are oriented such that, if pairs of intermolecular water−water contacts are treated as a single bridging unit, then this material adopts an ABX_3-type network in which the $[ZnCl_4]^{2-}$ fill the A-type void in the center of a $[Zn\{(OH_2)_2\}_{6/2}]^{2+}$ BX_3-type network, resulting in an antiperovskite structure type.

Notably, the adopted crystalline structure is intermediate between the ideal model limits of these more isotropic CsCl-type and ligand-close-packed-type structures. Shifting the observed triclinic lattice constants of a = 6.44 Å, b = 6.50 Å, c = 14.28 Å, α = 91°, β = 99°, and γ = 96° to lattice constants with $a = b = 0.5c$ and $\alpha = \beta = \gamma = 90°$ affords the ideal CsCl-type organization. By contrast, shifting the lattice constants to $a = b$ and $c = 4a \sin(70.53°/2)$, $\alpha = \beta = 90°$, and γ = 109.47° creates the ideal lattice for ligand cubic close packing (LCCP), which also affords the antiperovskite-type lattice. This LCCP lattice also corresponds to a cube with $a' = 2a \sin(109.47°/2)$, although the arrangement of the molecular ions in this cell does not exhibit cubic symmetry.

Structure of the Molten Salt Hydrate. As reviewed in the Introduction, the structure of molten zinc chloride hydrates has been a matter of significant interest for applied and fundamental scientific reasons.[24−33] Many previous reports suggest the prevalence of hexaaquozinc and/or tetrachlorozincate species in molten hydrates. However, to our knowledge, no reports have addressed exactly how these two

DOI: 10.1021/ic5024532
Inorg. Chem. 2015, 54, 1109−1119

molecular ions coexist in the liquids. Furthermore, a majority of analysis techniques provide only a picture of the averaged structure and thus apparent evidence of zinc coordination to both chloride and water. This resulted in the presumed existence and search for a variety of zinc chloride hydrate species, $[ZnCl_n(OH_2)_{4-n}]^{2-n}$ (n = 1−4) and/or $[ZnCl_n(OH_2)_{6-n}]^{2-n}$ (n = 0−4). When considered from a condensed-phase perspective, the stoichiometry limits the structural possibilities such that models with bridging chlorides to form oligomers have been proposed for concentrated zinc chloride hydrate solutions (R < 4).[24,26,30] The structural paradoxes of molten zinc chloride hydrates begin to be resolved with structural information from the crystal structure **I** for which it is demonstrated that (a) two nonequivalent zinc coordination environments can coexist, (b) $[Zn(OH_2)_6]^{2+}$ cations and $[ZnCl_4]^{2-}$ anions are the only species present, (c) zinc is coordinated to both chloride and water, just not in the same molecular-ion species, and (d) the low-water-content condensed phase is realized with a salt-like packing of distinct molecular ions rather than the formation of oligomeric zinc-chloride bridged species; albeit, oligomers are observed for the R = 1.33 structure.[40] It is important, then, to consider the extent to which the structure observed in the crystalline state is preserved in the liquid state.

The Raman spectrum of the R = 3 melt (Figure S4 in the SI), like that reported in the literature,[24−27] implies that, in the room temperature melt, both $[Zn(OH_2)_6]^{2+}$ and $[ZnCl_4]^{2-}$ are present. Stoichiometry requires that the existence of any additional "water of solution" would also require additional zinc chloride species. However, the exclusive coexistence of $[Zn(OH_2)_6]^{2+}$ and $[ZnCl_4]^{2-}$ in the R = 3 hydrate melt requires a salt-type packing of the ions.

PDF analysis of the synchrotron XRD and neutron diffraction of this molten salt hydrate along with a comparison to the PDFs of crystalline **I**, bulk water, and amorphous anhydrous $ZnCl_2$, as shown in Figure 5, provides additional insight into the liquid structure. Historically, the PDF data have been interpreted as providing evidence of both water and chloride coordination to zinc,[26,30−33] thus contradicting the interpretations of the Raman spectra because of the presumption of only a single coordination environment for zinc. However, with the crystalline structure of **I**, explicit definitions of individual pair correlations are possible, which can further be compared with the PDFs of the liquid. The partial PDFs calculated from the crystalline structure are given in Figure S6 in the SI. The smallest r peaks in the neutron PDF are the O−D and D−D pair correlations of the water molecules, which are not seen in the X-ray PDF. Notably, the feature at 1.8 Å in the neutron D_2O PDF, characteristic of the intermolecular hydrogen-bond distance of bulk water, is not observed in the R = 3 X-ray PDF. The smallest r peak that is common to both X-ray and neutron PDFs is at 2.24 Å, which is a combination of the shorter Zn−OH_2 and slightly longer Zn−Cl pair correlations, resulting in a distance slightly shorter than that observed for molten or glassy anhydrous $ZnCl_2$. It is important to recognize that PDF analysis does not discriminate between a case in which water and chloride are coordinated to the same zinc and one in which half the zincs are coordinated to water and the other half to chloride, and thus a weighted average distance is observed.

In both X-ray and neutron PDFs, there is a decrease in the number of pair correlations at 3.8 Å, assigned to Cl−Cl and Zn−Zn, with increasing amounts of hydration, i.e., $ZnCl_2$ > R = 1.72 > R = 3. The peaks at 3.2 and 4.3 Å in the X-ray PDF, which emerge in the molten hydrate, have historically been proposed as evidence of zinc chloride oligomers.[26] However, in light of pair correlations calculated from the single-crystal structure of **I**, we suggest these are more likely intra- and intermolecular ion O−O, Cl−O, Zn−Cl, and Zn−O contacts. These peaks are somewhat masked in the neutron PDF by overlapping D−Cl, D−O, D−D, and D−Zn correlations. The two broad peaks in the X-ray PDF between 5 and 8 Å, which are further broadened by the D−X pair correlations in the neutron PDF, are consistent with the pseudo-body-centered molecular cation−anion interactions and the pseudocubic molecular cation−cation and anion−anion correlations.

Raman and PDF analyses, which emphasize the local structure, give strong confirmation that the $[Zn(OH_2)_6]^{2+}$ and $[ZnCl_4]^{2-}$ ions persist into the liquid state. While the PDFs give an indication of intermolecular ion interactions, it is also important to consider the reciprocal space structure factor for evidence of any longer range ordering of these ions. In 1935, Prins, studying solutions of thorium and uranium nitrates by XRD, described the regular arrangement of ions in the liquid as giving rise to scattering consistent with a "superarrangement" analogous to a superlattice observed for some alloys.[48] Others too have observed that the low-angle diffraction peak(s) in the X-ray and neutron scattering of solutions is (are) indicative of a "quasi-close packing of solute ions".[49−51] Examination of the neutron structure factor plots for the crystalline and liquid samples of $\mathbf{I_D}$, in Figure 3b, demonstrates a high correlation between them, albeit with an expected lattice expansion, consistent with a lowering of the density from 2.13 g/cm^3 for crystalline $\mathbf{I_H}$ and 2.20 g/cm^3 for crystalline $\mathbf{I_D}$ to 1.93 and 1.98 g/cm^3, respectively, for their room temperature liquids, an 11% volume expansion.

Of particular note are the low-Q diffraction peak(s), whose origin has been the subject of considerable investigation, albeit with no clear interpretation, in anhydrous $ZnCl_2$ as well as other materials.[52] Unlike anhydrous $ZnCl_2$, where this low-Q peak is equivalent in both neutron and X-ray scattering, the R = 3 hydrate exhibits two distinct low-Q peaks at 0.81 and 1.23 Å^{-1} for neutron and X-ray scattering, respectively. Similarly distinct diffraction patterns are observed for neutron and X-ray patterns calculated for crystalline $\mathbf{I_D}$ and $\mathbf{I_H}$.

Shown in Figure 6 are the calculated crystalline neutron and X-ray patterns for the hypothetical structure of **I**, expanded such that the density matches the experimental liquid density and idealized to both the CsCl-type (a = 6.89 Å) and LCCP-type (a = 6.71 Å, c = 15.49 Å, or a' = 10.89 Å) lattices. These idealized and more isotropic structures simplify the diffraction patterns from that of the lower symmetry triclinic crystal and likely provide a better model of the liquid. Notably in both cases the low-Q features of the neutron patterns are the peaks corresponding to the edges of the pseudocubic CsCl-type box, (001) and (002), spacing between the respective cation and anion planes. By contrast, the low-Q X-ray scattering emphasizes the peaks corresponding to the face-centered layers, (101), (110), and (012), which each contain a mixture of anions and cations. The planes corresponding to ligand−ligand interactions, i.e., the height of the tetrahedron or octahedron, result in diffraction peaks with scattering around 2 ± 0.5 Å^{-1}.

The difference between the X-ray and neutron patterns is a result of the scattering power of the respective elements under the different types of radiation. In X-ray scattering, the

DOI: 10.1021/ic5024532
Inorg. Chem. 2015, 54, 1109−1119

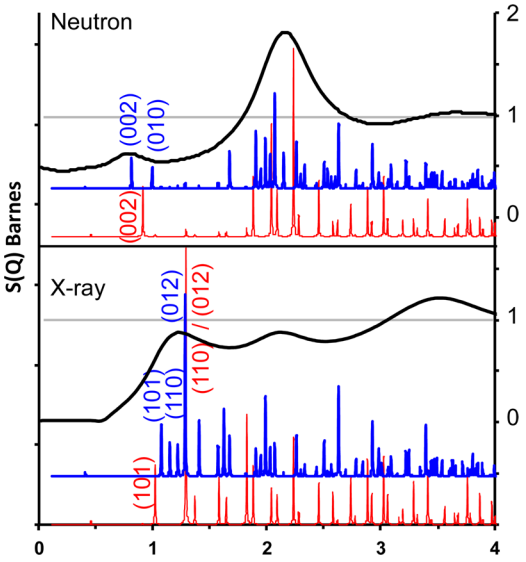

Figure 6. Low-Q portion of the experimental neutron and X-ray structure factor plots for the R = 3 room temperature liquid (black) compared with the respective calculated crystalline powder patterns for $\mathbf{I}_D$ neutron and $\mathbf{I}_H$ X-ray scattering for the CsCl-type (red) and LCCP-type (blue) lattices expanded to match the experimental liquid density.

scattering power scales with the number of electrons; thus, ZnO_6H_{12} exhibits 92% of the scattering of $ZnCl_4$. By contrast, the neutron scattering length cross sections (D, 6.7 fm; O, 5.8 fm; Cl, 9.6 fm; Zn, 5.6 fm) result in ZnO_6D_{12} exhibiting 275% of the scattering of $ZnCl_4$. As a result, cation−cation planes and any planes with water−water interactions will dominate neutron scattering, whereas X-ray scattering gives stronger weight to planes with anion−cation or Cl−Cl interactions.

Specifically, evaluation of the low-Q peaks from the calculated crystal structures allows evaluation of the CsCl- versus LCCP-type structures as models of the liquid structure. While the observed neutron low-Q peak of the R = 3 hydrate occurs at 0.81 $Å^{-1}$, the lowest peak with significant intensity in the CsCl-type structure occurs at 0.91 $Å^{-1}$. By contrast, the LCCP model indicates two peaks at 0.81 and 0.99 $Å^{-1}$, with the former being the most intense. The low-Q peak of the liquid X-ray pattern, at 1.23 $Å^{-1}$, is likely related to the dominant (012) peak at 1.28 $Å^{-1}$ for both structure types. However, its broadening to low Q with the {110} peaks in the LCCP model suggests that this model is more consistent with the observed liquid scattering than is the CsCl model in which the {110} and {012} peaks are equivalent. On the basis of that above, we propose that the distinct behavior of the low-Q liquid diffraction peaks with respect to neutron and X-ray scattering originate from lattice-type diffraction and systematic extinction conditions, and as such, the liquid most likely exhibits a disordered version of the LCCP structure that is dominated by ligand packing.

RMC Modeling. To gain further insight into this proposed ionic liquid structural model of the R = 3 hydrate, we performed a set of RMC calculations to fit the neutron scattering data. Structure factor, $S(Q)$, and PDF, $G(r)$, plots of these calculations are given in Figure 7. A simulation box was constructed by taking the pseudocubic set of four $\mathbf{I}_D$ unit cells ($2a \times 2b \times c$) and expanding them isotropically so as to match the experimental density. A molecular dynamics (MD) simulation was run on this expanded triclinic box to reassemble the molecular ions to reasonable metric parameters and to introduce disorder into the system. To also consider the CsCl- and LCCP-type structures, this MD box was idealized into a cubic modeling box (a = 13.8 Å) and a monoclinic box ($a = b$ = 6.71 Å, c = 15.49 Å, and γ = 109.47°), respectively. RMC modeling of 3 × 3 × 3 supercells of these boxes (equivalent to 108 $\mathbf{I}_D$ unit cells) was performed with intramolecular ion bond distances constrained to those of the above-characterized $[Zn(OD_2)_6]^{2+}$ and $[ZnCl_4]^{2-}$ ions.

The PDF of each of these simulations provides a remarkably good fit to the experimental PDF, with the only substantive difference between the calculated and experimental PDFs being observed for the intrawater D−D pair correlation at 1.47 Å, as seen in the inset of Figure 7. The MD and RMC components

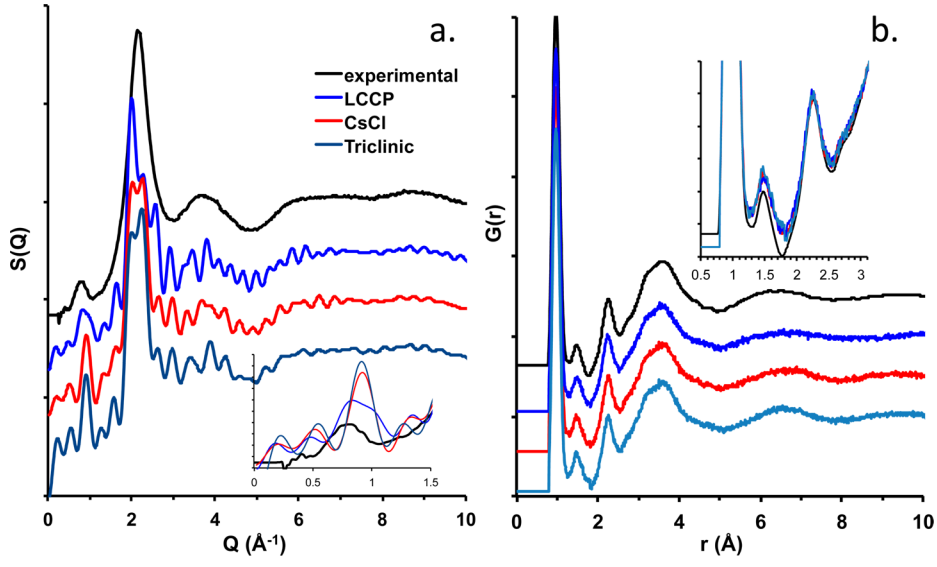

Figure 7. (a) Structure factor and (b) PDF plots comparing the experimental neutron scattering data for the R = 3 hydrate (black) with the RMC modeling of 5184-atom boxes based on the expanded triclinic (aqua), CsCl (red), and LCCP model structures. Inset in part a: expanded view of the low-Q peak. Inset in part b: 2× expanded view of the low-r PDF.

DOI: 10.1021/ic5024532
Inorg. Chem. 2015, 54, 1109−1119

of the simulation both introduce disorder into the system, but the overall crystal-type packing is clearly apparent, as observed in the LCCP simulation shown in Figure 8. While these simulated PDFs effectively replicate the local structure of the liquid, they do not provide sufficient detail to distinguish between the three simulation models.

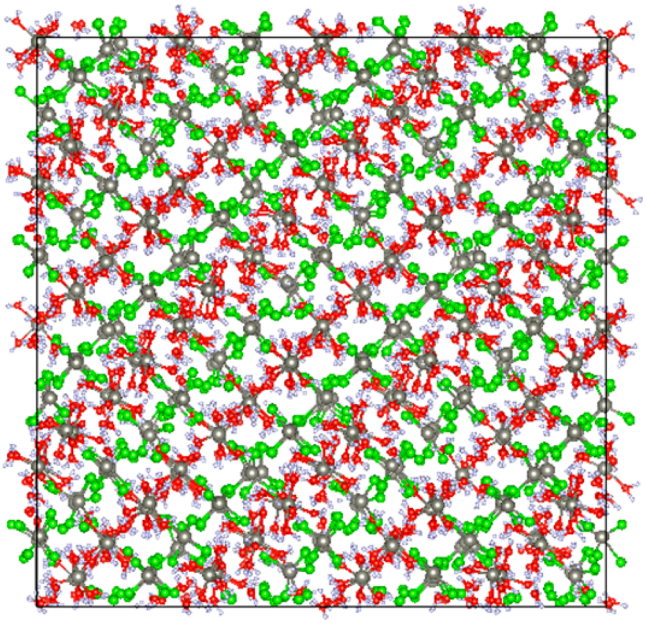

Figure 8. Ball-and-stick drawing of the RMC simulation box resulting from the LCCP model.

Somewhat greater structural insight is gained from the structure factor plots (Figure 7a). The structure factor plots from each of the models demonstrate that the diffraction patterns, while significantly broadened from those of the crystalline models, exhibit much more long-range order than is observed in the liquid. Nevertheless, the overall form of the simulation $S(Q)$ functions is consistent with the observed liquid scattering. Most significantly, however, the calculated position of the low-Q peak (see the inset of Figure 7a) is 0.91 $Å^{-1}$ for the triclinic simulation, 0.92 $Å^{-1}$ for the CsCl simulation, and 0.83 $Å^{-1}$ for the LCCP simulation. The LCCP model also exhibits a broadened and less intense peak than was observed for either the triclinic or CsCl models. This peak, along with the peak at 2 $Å^{-1}$, is extremely sensitive to the position of the water ligands and also the position of the D atoms relative to Zn−O. Thus, we propose that a more extensive disordering of the orientation of the water ligands of $[Zn(OD_2)_6]^{2+}$ is key to achieving a better model of the liquid structure. We suspect that the disordering of the water orientations is not completely random. Rather, as we demonstrated for the plastic crystalline CBr_4,[53] which like **I** must orient tetrahedra in an average cubic structure, there are likely a restricted set of possible orientations for the water ligands, defined by the overall LCCP-type packing.

Understanding the Water of Hydration. Examination of the IR spectrum (Figure 4) of the water of hydration provides important insight into the physical characteristics of this liquid that can be exploited for unique solvating properties. Unlike bulk water, the R = 3 hydrate exhibits only weak water−water and water−Cl hydrogen bonding. However, whereas strong hydrogen bonding in bulk water causes the ν_{OH} stretches (3363 cm^{-1}) to be significantly red-shifted from the resolved molecular symmetric and asymmetric stretches in the gas phase (3756 and 3652 cm^{-1}), the R = 3 hydrate still exhibits a major red shift in ν_{OH} to 3414 cm^{-1}, approximately 85% of the O−H bond weakening observed for the difference between the gas phase and bulk liquid water at room temperature. This is comparable (within 5%) to the OH stretch of bulk water at 91.1 °C.[54] However, in the R = 3 hydrate, the weakening of the O−H interactions is a result of O−H bond activation by coordination to the Lewis acidic Zn^{2+}. In a complementary fashion, the hydrogen-bonded network in bulk water strengthens the ν_{HOH} bend from the gas-phase value of 1595 cm^{-1} to 1638 cm^{-1}, whereas the more isolated coordinated water in the R = 3 hydrate exhibits an intermediate ν_{HOH} of 1617 cm^{-1}; this amounts to 51% of the difference between the molecular bend in the gas phase and the network-restricted bend in the room temperature bulk liquid. In addition, this red-shifted R = 3 ν_{HOH} peak is significantly sharpened, while its corresponding overtone observed at 3230 cm^{-1} is both red-shifted and diminished in intensity compared to that of bulk water, consistent with the oscillator becoming less strongly anharmonic as intermolecular hydrogen bonding is diminished. This contrasts with the behavior of ν_{HOH} and its overtone in bulk water at 91 °C, for which there is very little change to either.[54] The region assigned as the intramolecular bend overtone has also recently been suggested to be a result of intermolecular coupling.[47] Any intermolecular coupling in the liquid network would also be expected to diminish for the more isolated water molecules of the concentrated hydrate melt.

The much broader and weaker liberation + bend combination band, $\nu_{lib+HOH}$, exhibits a more dramatic change from that of bulk water (see the inset of Figure 4). This band is not observed in the gas-phase spectrum because it results from intermolecular bulk interactions. Upon dilution, this band at 2120 cm^{-1} in bulk water begins to shift to lower energy, becoming the band at 2000 cm^{-1} in the R = 3 liquid. The weakened ν_{HOH} cannot independently account for this substantial red shift, suggesting that ν_{lib} is also substantially weakened with the loss of intermolecular hydrogen bonding. By comparison, heating water from 31.0 to 91.1 °C only red-shifted this peak by 45 cm^{-1},[54] indicating that the water−water network interaction is much more disrupted in the R = 3 hydrate than in water near its boiling point. Furthermore, a second combination band to higher energy becomes visible with the addition of about 10 mol % $ZnCl_2$ (R = 9) and is clearly resolved at 2290 cm^{-1} in the R = 3 liquid. At the R = 3 composition, these two bands are approximately equal in intensity, with the new high-energy band surpassing the original lower-energy band in the R = 2 hydrate melt. We propose that this higher-energy band is a result of the restricted libration of water molecules tightly bound to zinc in the $[Zn(OH_2)_6]^{2+}$ cation in combination with ν_{HOH}.

Together, these IR data suggest that the water molecules in the R = 3 hydrate are substantially activated, and as such, they could be very strong hydrogen-bond donors. Such hydrogen bonding is not realized in the neat liquid because the $[ZnCl_4]^{2-}$ anion and the oxygen atoms of the water coordinated to zinc are poor hydrogen-bond acceptors. As a result, the untapped hydrogen-bond-donating capacity can likely be exploited toward hydrogen-bond-accepting solutes.

DOI: 10.1021/ic5024532
Inorg. Chem. 2015, 54, 1109−1119

CONCLUSION

This collection of thermodynamic, diffraction, and spectroscopic data clearly demonstrates the existence of the congruently melting zinc chloride trihydrate (R = 3) as a line phase. Solution of its single-crystal structure demonstrates that $[Zn(OH_2)_6][ZnCl_4]$ is rightly classified as a "zinc zincate" in which the two types of ligands, water and chloride ion, are associated with two different zinc atoms in strict segregation. Comparative analysis of the crystalline and liquid diffraction data, and the vibrational spectra of the liquid, all indicate that the pseudoligand ccp structure with a CsCl-type arrangement of the molecular ions of the R = 3 solid persists in its melt. As such, this hydrate melt is best described as a room temperature ionic liquid.

Vibrational spectroscopy demonstrates that, by sequestering the water molecules on the zinc ions, the O−H bonds are significantly activated such that they should be well suited to be hydrogen-bond donors. However, neither the zinc-bound oxygen atoms nor the tetrachlorozincate anion is an effective hydrogen-bond acceptor. The absence of significant intermolecular hydrogen bonding and the low charge density of the respective molecular ions are responsible for the observed low melting temperature of this "salt", as well as the melting point H/D inverse isotope effect.

Together, these features make the R = 3 hydrate a unique ionic liquid solvent. Notably neither ion of this molten hydrate exhibits a molecular dipole. As such, the packing of molecular ion monopoles in the liquid effectively makes this material a nonpolar solvent, albeit one that contains strong hydrogen-bond donors. We suggest that the historically documented solubility of cellulose in the R = 3 zinc chloride hydrate[2] provides an example of the unique solvating characteristics of this novel ionic liquid. The strong hydrogen-bond donation apparently disrupts the highly hydrogen-bond cross-linked network, while the nonpolar (monopolar) ionic liquid matrix stabilizes the isolated biopolymer molecules. Not only does this newly articulated structural description of the R = 3 zinc chloride hydrate ionic liquid provide an explanation to its physical properties, the impact of the network deconstruction on the IR spectrum of water provides a useful contribution to the ongoing effort to understand the structure of water, and the contrast between the neutron and X-ray scattering provides unprecedented insight into the origin of the low-Q diffraction peaks in liquids.

EXPERIMENTAL SECTION

Materials and Synthesis. Zinc chloride was purchased from Aldrich. The material was dried under a dynamic vacuum at 100 °C overnight and then sublimed. The purity of the starting material was confirmed to be anhydrous δ-$ZnCl_2$ by powder XRD and DSC (mp 317 °C). Purified $ZnCl_2$ was stored and utilized in a nitrogen-filled glovebox. 18 MΩ water was obtained from a Millipore Synergy ultrapure water filtration system. 99.99% D_2O was used as purchased from Aldrich.

DSC and capillary-scale samples were prepared by placing a sample (~20 mg) of δ-$ZnCl_2$ in a high-pressure stainless steel DSC pan, placed on the pan of a home-built environmentally controlled microbalance (the microbalance head was purchased from CI Electronics and is controlled by *LabWeigh* Software). A stream of nitrogen was passed through a water bubbler, and the saturated water vapor was passed over the sample until the desired stoichiometric amount of water had been sorbed. The hydration reaction was then stopped. Using a syringe with a 0.7-mm-i.d. fused-silica capillary affixed to the end, a 1−2 mm aliquot was drawn into the middle of the capillary, which was then flame-sealed on both ends of the zinc chloride hydrate sample. The DSC pan was then sealed using a gold seal. This preparation technique assured equivalent composition for structural and calorimetric measurements.

Bulk samples of $ZnCl_2{\cdot}3H_2O$ were prepared by adding, for example, 1.00 g of 18 MΩ H_2O (55.5 mmol) to 2.52 g of anhydrous $ZnCl_2$ (18.5 mmol). The samples were prepared and stored in Teflon-capped Pyrex vials. Solutions were mixed by agitation and equilibrated for a minimum of 2 days before any physical measurements were conducted.

Single-Crystal Structure. *$[Zn(OH_2)_6][ZnCl_4]$.* A 0.7-mm-i.d. capillary containing a 1 mm aliquot of the liquid $ZnCl_2{\cdot}3H_2O$ was affixed to a goniometer head on a Bruker AXS SMART APEX CCD diffractometer equipped with a Kryoflex cryostat. As a representative example, a crystal was grown from the melt by rapid cooling of the capillary to a −50 °C isotherm in the cryostat's cold stream. The sample was held at the crystallization isotherm for 1 h to afford crystallization. The sample was then further cooled to 208 K for data collection. Single or near-single crystal(s) were obtained, and the lattice constants were measured. The best crystal was selected based on the diffraction pattern using the program *Cell Now*. The selected domain accounted for the most intense reflections, for all high-angle reflections, and for about half of all harvested reflections. Other domains were ignored during the integration, and all reflections were used, regardless of overlap with reflections from other domains. Reflections were collected from an entire Ewald sphere with 5738 unique reflections measured for 2.88° < 2θ < 56.56°. The final unit cell determination and structural refinement were made using a symmetry-constrained fit of 2868 reflections. The data were corrected for absorption using *SADABS*. The structure was solved by direct methods and refined by full-matrix least squares against F^2 with all reflections using *SHELXL-97* (Sheldrik 2008, Bruker 2000−2003).

$[Zn(OD_2)_6][ZnCl_4]$. A 0.5-mm-i.d. capillary containing a 1 mm aliquot of liquid $ZnCl_2{\cdot}3H_2O$ was affixed to a goniometer head and placed directly in the cold stream at 253 K on a Bruker-Nonius Kappa Axis X8 Apex 2 diffractometer with an Oxford Cryosystems 700 cryostat. The sample was further cooled to 233 K at a rate of 360 K/h. A near-single crystal was observed to have grown after 10 min at the 233 K isotherm. Unit cell determination and indexing were performed on the dominant domain, which could be treated as a single crystal. Reflections were collected from an entire Ewald sphere with 5799 unique reflections measured for 5.78° < 2θ < 73.04°. The final unit cell determination and structural refinement were made using all unique reflections. The data were corrected for absorption using *SADABS*. The structure was solved by direct methods and refined by full-matrix least squares against F^2 with all reflections using *SHELXL-2014* (Sheldrik 2014).

Synchrotron XRD of the Liquid. A 0.7-mm-i.d. capillary containing a 1−2 mm aliquot of molten $ZnCl_3{\cdot}3H_2O$ was affixed to a goniometer head on the diffractometer on line 11-ID-B at the Advanced Photon Light Source, Argonne National Laboratory. The sample was measured at room temperature, ~295 K. A 90 keV (λ = 0.13702 nm) X-ray beam was utilized to collect an average of 100 scans at 10 s/scan using a GE amorphous silicon detector. Data for background subtraction were obtained using the same sample capillary that was shifted such that no sample, only the fused silica capillary, was in the beam. The raw two-dimensional data were radially integrated using *Fit2D*.[55] The diffraction data were subsequently transformed into a structure factor $S(Q)$, subtracting the background and correcting the data for sample and instrument effects such as Compton scattering, Laue diffuse scattering, self-absorption, X-ray polarization, and the scattering based on the elements present. Transformation of the data to obtain $S(Q)$ and its inverse Fourier transform PDF $G(r)$ was performed using the *PDFgetX2* program.[56]

Neutron Diffraction. Samples of 1 mL were sealed into 5-mm-o.d. quartz NMR tubes (WILMAD). The samples as well as an empty NMR tube were mounted on the linear sample changer installed at the NOMAD diffractometer, Spallation Neutron Source, Oak Ridge National Laboratory.[57] The linear sample changer was equipped with a Cobra Plus Cryosystem from Oxford modified for use with

DOI: 10.1021/ic5024532
Inorg. Chem. 2015, 54, 1109−1119

neutron scattering to operate with temperature-controlled argon gas. Argon gas has a very small neutron scattering cross section and, hence, a considerably reduced background contribution compared to the more commonly used dinitrogen. The neutron event data were binned as a function of Q using a calibration derived from measurement of the diamond powder, as described in ref 57 and normalized to the integrated proton charge accumulated on the neutron target. Measurements obtained from a 5.8-mm-diameter vanadium rod were used for normalization of the sample data to a differential cross section. The incoherent contribution to the scattering cross section was approximated by a pseudo-Voigt function. Data were collected to Q_{max} = 50 Å^{-1}. On the basis of the total scattering the structure factor $S(Q)$, the reduced atomic PDF $G(r)$ was calculated using data up to Q = 31 Å^{-1}. Data were collected from 100 to 333 K for specific isotherms (sum of three 20 min scans) or with a ramped temperature profile 1 or 5 °C/min. Transformation of the data to obtain $S(Q)$ and its inverse Fourier transform PDF $G(r)$ was performed using the *NOMAD-SNS* analysis suite of programs.

GSAS Structural Determination. The structure refinement for one sample was performed using *GSAS* and *EXPGUI* software.[58] The sample was obtained by cooling 0.5 mL of a R = 3 hydrate melt to 225 K at a rate of 0.5 °C/min. The structure was refined against the neutron time-of-flight (TOF) data from one of six detector banks on the NOMAD instrument. The background of the TOF data, lattice parameters, atomic coordinates, occupancies, and atomic displacement parameters were refined.

ATR-IR. IR spectra were collected using a Digilab FTS-3000 Fourier transform IR spectrometer using a mounted crystalline germanium, ATR sampling attachment (Pike TechnologiesIinc., MIRacle Single Reflection ATR) with a normal spectral response of 650−5500 cm^{-1}. A droplet of the molten hydrate (or 18 MΩ H_2O) was pipetted onto the ATR crystal and the crystal element capped. The IR light was focused onto the photodiode of a liquid-nitrogen-cooled, narrow-band mercury−cadmium−telluride detector with a normal spectral response of 650−7000 cm^{-1}. There is nominally one reflection with a spot size of approximately 100 μm. The spectrometer was purged with dry nitrogen, which reduces atmospheric water or CO_2 contamination in the spectral beam path. Spectra were recorded at room temperature, approximately 23 ± 0.5 °C with a resolution of 1 cm^{-1}. The spectra were converted into absorbance units by taking the negative of the log ratio of a sample spectrum to that of an empty crystal.

Raman. Approximately 0.5 mL samples of the liquid zinc chloride hydrate were placed into a septum-capped 5 mm NMR tube and spun with an air piston spinning sample holder. Raman spectra were collected using a Spex 1877E Triplemate monochromator fitted with a liquid-nitrogen-cooled CCD detector. The primary light source for excitation is a frequency-doubled Coherent Mira 900 Ti:sapphire laser system, which consists of a Coherent Verdi (10W) pump laser, a Coherent Mira 900 Ti:sapphire laser used to generate 532 nm light, and an Inrad 5-050 Ultrafast Harmonic Generation system to generate 406 nm light. The output light of the Ti:sapphire laser system was used as the excitation source for all Raman experiments, with a typical energy of 60 mW at the sample. All spectra were recorded at room temperature, approximately 23 ± 0.5 °C. The sample Raman spectra's were calibrated using the known spectral bands of carbon tetrachloride, indene, toluene, and cyclohexane by plotting the observed peak locations against their known positions. The plot was then fitted to a line, the slope of which was used to correct the X-axis of the sample spectra.

Computational Methods. *MD.* MD was performed in order to obtain the starting configuration required for the RMC modeling.[59] The MD simulations were performed using the *CPMD* package.[60] The plane wave/pseudopotential method was employed. The basis set energy cutoff was set to 60 Ry. The Troullier−Martins pseudopotential[61] with the PBE functional[62] was employed for electronic structure calculations. The starting configuration for the MD simulation originated from the crystal structure $\mathbf{I_D}$. Initially, the lattice parameters of the crystal structure were expanded to 6.7075, 6.7400, and 14.811 Å and 90.656°, 98.936°, and 95.498° in order to match the experimentally measured density of 1.98 g/mL for the liquid. The cell was then extended to a 2 × 2 × 1 supercell containing 192 atoms. Car−Parrinello MD[63] was performed on this supercell. The total simulation time was 1.56 ps using 0.12 fs timesteps. The Nosé−Hoover thermostat[64] was employed with a coupling frequency of 3000 cm^{-1} and a constant temperature of 298 K. The nuclear configuration at the last time step (i.e., 1.56 ps) was taken as the starting configuration for RMC.

RMC. RMC modeling was performed using *RMCProfile*[65] in order to obtain a model of the liquid system. Distance window constraints, acting as a hard-sphere potential, were set equivalent to the width of the intramolecular ion-pair correlations to allow for additional variation in the liquid. Refinement of the structure was performed simultaneously for both $S(Q)$ and $G(r)$ data obtained at ∼298 K from *NOMAD* for a R = 3 zinc chloride hydrate sample. Each simulation box contained 5184 atoms, and the calculations were run for between 5 and 50 h.

■ ASSOCIATED CONTENT

Supporting Information

X-ray crystallographic files in CIF format for the four X-ray single-crystal refinements and the GSAS refinement of neutron data, temperature dependence of the unit cell volume of **I** (Figure S1), GSAS refinement of $\mathbf{I_D}$ (Figure S2), variable-temperature neutron diffraction of the R = 3 hydrate (Figure S3), Raman spectra (Figure S4), drawings of pseudo-close-packed ligand planes (Figure S5), and calculated partial pair correlations (Figure S6). This material is available free of charge via the Internet at http://pubs.acs.org.

■ AUTHOR INFORMATION

Corresponding Author

*E-mail: Jim_Martin@NCSU.edu

Notes

The authors declare no competing financial interest.

■ ACKNOWLEDGMENTS

This work was supported by NSF Grant DMR-0705190 and ACS-PRF Grant 46439-AC10. Research conducted at ORNL's Spallation Neutron Source was sponsored by the Scientific User Facilities Division, Office of Basic Energy Sciences, U.S. Department of Energy (DOE), with assistance from Dr. Jöerg Neuefeind, Dr. Mikhail Feygenson, and John Carruth. Use of the Advanced Photon Source, Argonne National Laboratory, was supported by the Office of Science User Facilities operated for the DOE, Office of Science, under Contract DE-AC02-06CH11357 with support from beamline scientists Dr. Peter Chupas and Dr. Karina Chapman. The ATR-IR and Raman spectroscopy data were collected at the Laser Imaging and Vibrational Spectroscopy Facility located at North Carolina State University in the Department of Chemistry with the assistance of Dr. Simon Lappi. The X-ray diffractometer at Youngstown State University was funded by NSF Grant 0087210, Ohio Board of Regents Grant CAP-491, and Youngstown State University.

■ DEDICATION

This work is dedicated to the memory of Professor John D. Corbett, with whom J.D.M. had the privilege to work as a postdoctoral fellow. John had worked on the chemistry of zinc chloride, specifically working to understand the equilibrium structure of ZnCl(g).[66] When J.D.M. began working on $ZnCl_2$, John warned that this material is plagued with complication because of its extreme hygroscopic character. It is thus fitting to

DOI: 10.1021/ic5024532
Inorg. Chem. 2015, 54, 1109−1119

dedicate this contribution to resolving a portion of zinc chloride's hydration chemistry to his memory.

REFERENCES

(1) Taylor, T. English Patent 787, 1859.
(2) Barnes, H. L.; Rose, A. W. *Science* **1998**, *279*, 2064−2065.
(3) Crerar, D.; Wood, S.; Brantley, S.; Bocarsly, A. *Can. Mineral.* **1985**, *23*, 333−352.
(4) Beck, F.; Rüetschi, P. *Electrochim. Acta* **2000**, *45*, 2467−2482.
(5) Nicholson, J. W.; Parker, L. *J. Mater. Sci.* **1998**, *33*, 2251−2254.
(6) Christianson, D. W. *Adv. Protein Chem.* **1991**, *42*, 281.
(7) Prasad, A. S. *Ann. Intern. Med.* **1996**, *125*, 142−144.
(8) Braunstein, J. *Inorg. Chim. Acta, Rev.* **1968**, *2*, 19−30.
(9) Mylius, F.; Dietz, R. *Z. Anorg. Chem.* **1905**, *44*, 209−220.
(10) Angell, C. A.; Sare, E. J. *J. Chem. Phys.* **1970**, *52*, 1058−1068.
(11) Harris, A. C.; Parton, H. N. *Trans. Faraday Soc.* **1940**, *36*, 1139−1141.
(12) Foxton, F; Shutt, W. J. *Trans. Faraday Soc.* **1927**, *23*, 480−488.
(13) Robinson, R. A.; Stokes, R. H. *Trans. Faraday Soc.* **1940**, *36*, 740−748.
(14) Lutfullah, B.; Dunsmore, H. S.; Paterson, R. *J. Chem. Soc., Faraday Trans. 1* **1976**, *72*, 495−503.
(15) Goldberg, R. N. *J. Phys. Chem. Ref. Data* **1981**, *10*, 1−55.
(16) Hittorf, W. *Z. Phys. Chem.* **1903**, *43*, 239−249.
(17) Rabinowitsch, A. J. *Z. Phys. Chem.* **1921**, *99*, 338−360.
(18) Mead, D. J.; Fuoss, R. F. *J. Phys. Chem.* **1945**, *49*, 480−482.
(19) Easteal, A. J.; Sare, E. J.; Moynihan, C. T.; Angell, C. A *J. Solution Chem.* **1974**, *3*, 807−821.
(20) Agnew, A.; Paterson, R. *J. Chem. Soc., Faraday Trans.* **1978**, *74*, 2896−2906.
(21) Miller, D. G.; Rard, J. A. *J. Mol. Liq.* **1992**, *52*, 145−179.
(22) Thomas, B. K.; Fray, D. J. *J. Appl. Electrochem.* **1982**, *12*, 1−5.
(23) Nakamura, Y.; Shimokawa, S.; Futamata, K.; Shimoji, M. *J. Chem. Phys.* **1982**, *77*, 3258−3262.
(24) Irish, D. E.; McCarroll, B.; Young, T. F. *J. Chem. Phys.* **1963**, *39*, 3436−3444.
(25) Morris, D. F. C.; Short, E. L.; Waters, D. N. *J. Inorg. Nucl. Chem.* **1963**, *25*, 975−983.
(26) Yamaguchi, T.; Hayashi, S.; Ohtaki, H. *J. Phys. Chem.* **1989**, *93*, 2620−2625.
(27) Kanno, H.; Hiraishi, J. *J. Raman Spectrosc.* **1980**, *9*, 85−89.
(28) Mayanovic, R. A.; Anderson, A. J.; Bassett, W. A.; Chou, I.-M. *J. Synchrotron Radiat.* **1999**, *6*, 195−197.
(29) Matsubara, E.; Waseda, Y. *J. Phys: Condens. Matter* **1989**, *1*, 8575−8582.
(30) Kruh, R. F; Standley, C. L. *Inorg. Chem.* **1962**, *1*, 941−942.
(31) Wertz, D. L.; Bell, J. R. *J. Inorg. Nucl. Chem.* **1973**, *35*, 861−868.
(32) Paschina, G.; Piccaluga, G.; Pinna, G.; Magini, M. *J. Phys. Chem.* **1983**, *78*, 5745−5749.
(33) Powell, D. H.; Barnes, A. C.; Enderby, J. E.; Neilson, G. W.; Salmon, P. S. *Faraday Discuss. Chem. Soc.* **1988**, *85*, 137−146.
(34) Parchment, O. G.; Vincent, M. A.; Hillier, I. H. *J. Phys. Chem.* **1986**, *100*, 9689−9693.
(35) Tossell, J. A. *J. Phys. Chem.* **1991**, *95*, 366−371.
(36) Rudolph, W. W.; Pye, C. C. *Phys. Chem. Chem. Phys.* **1999**, *1*, 4583−4593.
(37) Brehler, B.; Jacobi, H. *Naturwissenschaften* **1964**, *51*, 11.
(38) Brehler, B; Süsse, P. *Naturwissenschaften* **1963**, *50*, 517.
(39) Liu, Xi; Guo, G.-C.; Sun, Y. Y. *Acta Crystallogr., Sect. E: Struct. Rep. Online* **2007**, *63*, m275.
(40) Follner, v. H.; Brehler, B. *Acta Crystallogr.* **1970**, *B26*, 1679−1682.
(41) Martin, J. D.; Goettler, S. J.; Fosse, N.; Iton, L. *Nature* **2002**, *419*, 381−384.
(42) Martin, J. D.; Keary, C. L.; Thornton, T. A.; Novotnak, M. P.; Knutson, J. W.; Folmer, J. C. W. *Nat. Mater.* **2006**, *5*, 271−275.
(43) Josey, A. A. Thesis, North Carolina State University, Raleigh, NC, 2008
(44) Hou, F.; Martin, J. D., Dill, E. D.; Josey, A. A.; Folmer, J. C. W. Manuscript in preparation.
(45) Duhlev, R; Macicek, J. *Acta Crystallogr., Sect. C* **1991**, *47*, 1573−1575.
(46) Soper, A. K. *J. Phys: Condens. Matter* **2007**, *19*, 335206(18pp).
(47) Shi, L; Gruenbaum, S. M.; Skinner, J. L. *J. Phys. Chem. B* **2012**, *116*, 13821−13830.
(48) Prins, J. A. *J. Chem. Phys.* **1935**, *3*, 72−80.
(49) Alves Marques, M.; Cabaco, M. I.; de Barros Marques, M. I.; Gaspar, A. M. *J. Phys: Condens. Matter* **2002**, *14*, 7427−7448.
(50) Angell, C. A.; Byrne, N.; Belieres, J.-P. *Acc. Chem. Res.* **2007**, *40*, 1228−1236.
(51) Matsubara, E.; Waseda, Y. *J. Phys.: Condens. Matter* **1989**, *1*, 8575−8582.
(52) Wright, A. C. *Glass Phys. Chem.* **1998**, *24*, 148−179.
(53) Folmer, J. C. W.; Withers, R. L.; Welberry, T. R.; Martin, J. D. *Phys. Rev. B* **2008**, *77* (144205), 1−10.
(54) Larouche, P.; Max, J.-J.; Chapados, C. *J. Chem. Phys.* **2008**, *129*, 064503−1−13.
(55) Software available at www.esrf.eu/computing/scientific/FIT2D/ .
(56) Qiu, X.; Thompson, J. W.; Billinge, S. J. L. *J. Appl. Crystallogr.* **2004**, *37*, 678.
(57) Neuefeind, J.; Feygenson, M.; Carruth, J.; Hoffmann, R.; Chipley, K. *Nucl. Instrum. Methods Phys. Res., Sect. B* **2012**, *287*, 68−75.
(58) (a) Larson, A. C.; Von Dreele, R. B. *General Structure Analysis System (GSAS); LAUR 86-748*; Los Alamos National Laboratory: Los Alamos, NM, 2000. (b) Toby, B. H. *J. Appl. Crystallogr.* **2001**, *34*, 210−213.
(59) McGreevy, R. L.; Pusztai, L. *Mol. Simul.* **1988**, *1*, 359−367.
(60) *CPMD*, version 3.17.1; see http://www.cpmd.org/.
(61) Troullier, N.; Martins, J. L. *Phys. Rev. B* **1991**, *43*, 1993−2006.
(62) Perdew, J. P.; Burke, K.; Ernzerhof, M. *Phys. Rev. Lett.* **1996**, *77*, 3865−3868.
(63) Car, R.; Parinello, M. *Phys. Rev. Lett.* **1985**, *55*, 2471−2474.
(64) (a) Nosé, S. *J. Chem. Phys.* **1984**, *81*, 511−519. (b) Hoover, W. G. *Phys. Rev. A* **1985**, *31*, 1695−1697. (c) Tucker, M. G.; Keen, D. A.; Dove, M. T.; Goodwin, A. L.; Hui, Q. *J. Phys.: Condens. Matter* **2007**, *19*, 335218.
(65) Tucker, M. G.; Keen, D. A.; Dove, M. T.; Goodwin, A. L.; Hui, Q. *J. Phys.: Condens. Matter* **2007**, *19*, 335218.
(66) Corbett, J. D.; Lynde, R. A. *Inorg. Chem.* **1967**, *6*, 2199−2204.

DOI: 10.1021/ic5024532
Inorg. Chem. 2015, 54, 1109−1119